FINITE ELEMENT ANALYSIS ON THE SINTERING OF STAINLESS STEEEL 316L POWDER COMPACTS

Rui Zhang, Renata S. Engel,
Nicholas J. Salamon, and Randall M. German

Center for Innovative Sintered Products (CISP)
P/M Lab, 147 Research West
The Pennsylvania State University
University Park, PA 16802

ABSTRACT

Implementation of an accurate sintering model into a finite element simulation program can significantly improve Powder Metallurgy (P/M) part properties and processing efficiency. The densification and creep behavior of stainless steel powders during free sintering has been simulated and the material model has been implemented by linking user subroutines to the ABAQUS finite element code. This approach is based upon the continuum theories of elastic and nonlinear-viscous deformation of porous bodies. The nonuniform density distribution of the green compact is considered as an initial condition for the FEM model. The porosity is updated during the simulation. Grain growth, gravity, thermal expansion, thermal conductivity, and other heterogeneous factors are also considered during the simulation. Several applications with different powder size range have been performed and the simulation results of axial shrinkage and density distribution changes have been compared before and after sintering. Dilatometry tests have been performed to validate the simulation results.

INTRODUCTION

Die pressing of the powder and sintering of the powder compact are the economically most important methods for P/M products. Due to the variation of cross-section of a compact and the friction effect, die pressing usually results in an inhomogeneous density distribution which causes shape distortions of the part during sintering. Since hard machining of the sintered parts is expensive, one of the main goals in the industrial production process is the optimization of the processing route with respect to the geometry of the as-sintered part. Compared with the empirical optimization, numerical simulation is much less expensive and saves a lot of time, especially for a newly designed product.

In order to simulate the sintering process using finite element method, a basic material continuity assumption has to be set. Several constitutive laws based upon the continuum theories have been developed for modeling of sintering, e.g. Riedel[1] (1990), Olevsky[2] (1998). Many groups have modeled the sintering process, e.g. Sun & Riedel[3] (1995), Zipse[4] (1997), Kim and Jeon[5] (1998), Gillia and Bouvard[6] (1998), Gasik and Zhang[7] (2000).

The main purpose of the present paper is to describe a feasibility study to model the sintering process with consideration of most of the heterogeneous factors, especially the inhomogeneous density distribution from die compaction process. Compared with the dilatometer data, the simulation results of axial shrinkage are reasonable. The changing of density distribution due to a prescribed initial condition has been achieved.

CONSTITUTIVE LAW

For the phenomenological model of sintering, the constitutive equation is selected as a linear-viscous incompressible model containing isotropically distributed voids. The strain rate is comprised of the elastic strain rate $\dot{\boldsymbol{\varepsilon}}^{e}$, thermal strain rate $\dot{\boldsymbol{\varepsilon}}^{t}$, and viscoplastic (creep) strain rate $\dot{\boldsymbol{\varepsilon}}^{cr}$.

$$\dot{\boldsymbol{\varepsilon}} = \dot{\boldsymbol{\varepsilon}}^{e} + \dot{\boldsymbol{\varepsilon}}^{t} + \dot{\boldsymbol{\varepsilon}}^{cr} \tag{1}$$

The portion of elastic strain rate is assumed as linear and isotropic, which can be expressed by a rate form of Hooke's law,

$$\dot{\boldsymbol{\sigma}} = \mathbf{C}\dot{\boldsymbol{\varepsilon}}^{e} = \mathbf{C}\left(\dot{\boldsymbol{\varepsilon}} - \dot{\boldsymbol{\varepsilon}}^{t} - \dot{\boldsymbol{\varepsilon}}^{cr}\right) \tag{2}$$

where $\mathbf{C}$ is called isotropic elasticity tensor. The thermal strain rate is caused by thermal expansion which can be expressed as:

$$\dot{\boldsymbol{\varepsilon}}^{t} = \alpha \Delta T \mathbf{I} \tag{3}$$

where α is the coefficient of thermal expansion, ΔT is the increment of temperature, $\mathbf{I}$ is the unit matrix. The viscoplastic (creep) strain rate obeys a linear-viscous law[8] that has the following form,

$$\dot{\boldsymbol{\varepsilon}}^{cr} = \frac{\boldsymbol{\sigma}'}{2G} + \frac{\mathrm{tr}(\boldsymbol{\sigma}) - 3\sigma_s}{9K}\mathbf{I} \tag{4}$$

where $\boldsymbol{\sigma}'$ is the deviatoric stress, G is the shear viscosity modulus, K is the bulk viscosity modulus, $\mathrm{tr}(\boldsymbol{\sigma})$ is the trace of the stress tensor, and σ_s is the sintering stress (the equivalent hydrostatic pressure caused by local capillary stresses in porous structures). The effective Laplace pressure (sintering stress) is

$$P_L = \sigma_s = \frac{\partial F}{\partial V_T} \tag{5}$$

where F is the free energy per unit mass of porous medium, V_T is the total volume per unit mass. It is shown [2] that

$$\sigma_s = \frac{3\omega}{r_0}(1-\theta)^2 \tag{6}$$

where r_0 is the mean radius of powder particles and ω is a surface tension. The porosity θ is defined as the ratio of the volume of pores to the total volume:

$$\theta = \frac{V_{pores}}{V_{total}} \tag{7}$$

The apparent viscosity for stainless steel 316L and 17-4PH powders is calculated [9] as

$$\eta = \eta_0 \exp\left(\frac{Q}{RT}\right) \tag{12}$$

where η_0 is a coefficient of viscosity which usually falls in the range of 130~140 GPa·s; Q is the activation energy which is equal to 20.0 kJ/mol[10] and R is, the universal gas constant, 8.314 J/K·mol.

For G and K in equation (4), it is shown [2] that:

$$G = (1-\theta)^2 \eta \tag{8}$$

$$K = \frac{4}{3}\frac{(1-\theta)^3}{\theta}\eta \tag{9}$$

APPLICATION IN ABAQUS

In this paper, ABAQUS standard 6.2 is used as finite element solver. In order to achieve the constitutive law described above, subroutine CREEP is used. For metals, the ABAQUS[11] routine for incremental creep strain (the incremental viscoplastic strain) allows the swelling and creep components to be defined as

$$\Delta\hat{\boldsymbol{\varepsilon}}^{cr} = \frac{1}{3}\Delta\bar{\varepsilon}^{sw}\mathbf{R} + \Delta\bar{\varepsilon}^{cr}\mathbf{n} \tag{13}$$

where $\Delta\bar{\varepsilon}^{sw}$ and $\Delta\bar{\varepsilon}^{cr}$ are the incremental volumetric swelling strain and the uniaxial equivalent "creep" strain, respectively. **R**=**I** for isotropic swelling and **n** is the gradient of the deviatoric stress potential, defined as

$$\mathbf{n} = \frac{\partial\tilde{q}}{\partial\boldsymbol{\sigma}} = \frac{3\boldsymbol{\sigma}'}{2\tilde{q}} \tag{14}$$

where the deviatoric stress $\boldsymbol{\sigma}' = \boldsymbol{\sigma} + p\mathbf{I}$, and $\tilde{q}$ is the Mises equivalent deviatoric stress given by

$$\tilde{q} = \sqrt{\frac{3}{2}\boldsymbol{\sigma}'\boldsymbol{\sigma}'} \tag{15}$$

From equation (4), the incremental form of the creep strain can be expressed as:

$$\Delta\hat{\boldsymbol{\varepsilon}}^{cr} = \frac{\mathrm{tr}(\boldsymbol{\sigma})\Delta t - 3\sigma_s\Delta t}{9K}\mathbf{I} + \frac{\boldsymbol{\sigma}'\Delta t}{2G} \tag{16}$$

Comparison of (13) and (16) leads to the connections:

$$\frac{\mathrm{tr}(\boldsymbol{\sigma})\Delta t - 3\sigma_s \Delta t}{9K}\mathbf{I} = \frac{1}{3}\Delta\bar{\varepsilon}^{sw}\mathbf{R} \tag{17}$$

$$\frac{\boldsymbol{\sigma}'\Delta t}{2G} = \Delta\bar{\varepsilon}^{cr}\mathbf{n} = \Delta\bar{\varepsilon}^{cr}\frac{3\boldsymbol{\sigma}'}{2\tilde{q}} \tag{18}$$

Hence the incremental creep strain components can be expressed as:

$$\Delta\bar{\varepsilon}^{sw} = \frac{\mathrm{tr}(\boldsymbol{\sigma}) - 3\sigma_s}{3K}\Delta t = -\frac{p + \sigma_s}{K}\Delta t \tag{19}$$

$$\Delta\bar{\varepsilon}^{cr} = \frac{\tilde{q}}{3G}\Delta t \tag{20}$$

where $p = -\frac{1}{3}\mathrm{tr}(\boldsymbol{\sigma})$ is the equivalent pressure stress.

In the above derivation, G and K are both functions of porosity. Hence for finite deformation, it is important to update porosity during the simulation process. By assuming the balance of mass in both compaction and sintering processes, the porosity θ can be expressed as a function of strain components at each material point.

In ABAQUS, logarithmic strain will be used for geometrically nonlinear analysis. The definition of logarithmic strain is

$$\varepsilon^{l} = \int_0^t \frac{dL}{L} = \ln L\Big|_{L_0}^{L} = \ln\frac{L}{L_0} \tag{21}$$

where L_0 is the initial length and L is the current length in a one-dimensional case. Accordingly, the relative density can be described in term of the logarithmic strain components as in the following equation:

$$\rho = \rho_0 \exp(-\varepsilon_{kk}) \tag{22}$$

where ρ_0 is the initial density, ρ is the final density, ε_{kk} is the volume strain in 3D case. In CREEP subroutine of ABAQUS, ε_{kk} is equal to the swelling strain $\bar{\varepsilon}^{sw}$.

SAMPLE PREPARATION AND EXPERIMENT

Three groups of SS316L powder, SS316L-Small, Medium and Large, have been sieved from one source powder. The particle size can be seen in Fig 1. Table 1 shows the effect of particle size on material properties. The SS 316L-small group has the highest *Hausner Ratio*, which means most irregular particle shape, and highest compressibility. In the die compaction process, it can also be found that, in order to get

the same green density, pressure needed by the SS316L-Small group is smaller than those needed by the other two groups.

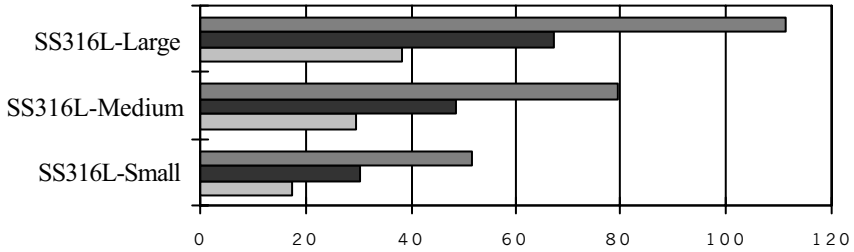

	SS316L-Small	SS316L-Medium	SS316L-Large
D90	52.047	79.566	111.241
D50	30.405	48.82	67.508
D10	17.262	29.502	38.384

Powder size(micron)

Fig.1 Density distribution for sieved stainless steel 316L powders

For each group of powder, the considered one-punch pressed green part is in the shape of cylinder. The bulk density is around 82%. The diameter is 12.58 mm and the height is 12.08mm in the green state. The sample has 0.5wt% Acrowax as lubricant, debound at 450°C for 2 hours and presintered at 900°C for 30 minutes, followed by sintering in dilatometer at 1350°C for 1 hour. The shrinkage curves are recorded during the dilatometer tests as shown in Fig.2. The final axial shrinkages are: small size---3.16%, middle size---2.53%, and large size---2.01%. There is a 57% increase from the small size to large size particle compacts.

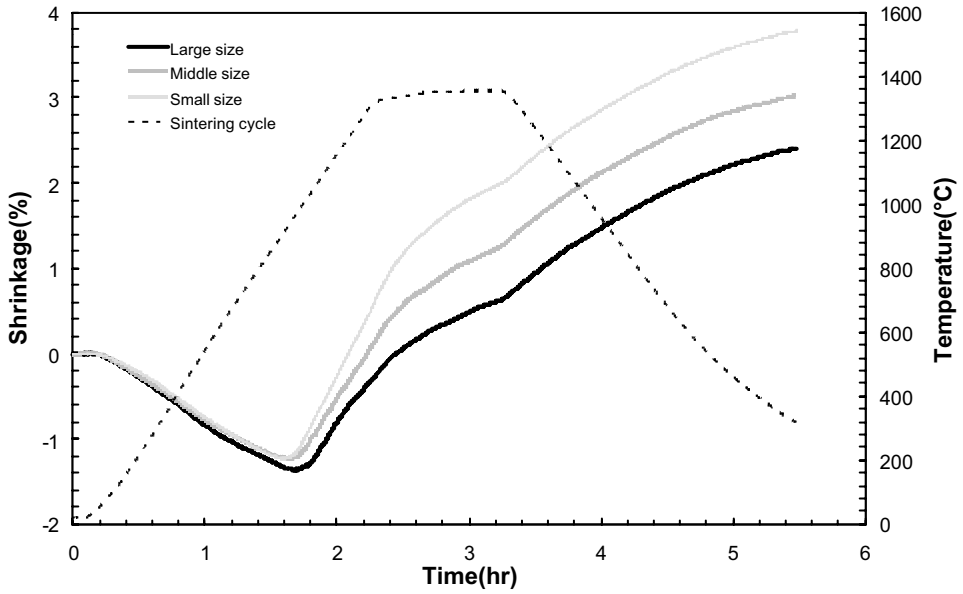

Fig.2 Dilatometer plots of axial shrinkage versus time for three stainless steel 316L presintered compacts with different particle size heated at a rate of 10°C/min to 1350°C in hydrogen

Table 1. Apparent and tap densities of water-atomized SS 316L as affected by powder particle size

Powder	Mean size (μm)	Apparent Density (d_a) (g/cm^3)	Tap Density (d_f) (g/cm^3)	Hausner Ratio (d_f/d_a)	Pycnometer Density (g/cm^3)
SS316L-Large	72.526	2.22	3.41	1.5370	7.85
SS316L-Medium	52.528	2.36	3.66	1.5376	7.85
SS316L-Small	33.389	2.41	3.87	1.6087	7.91

FINITE ELEMENT MODEL

A two dimensional model is made for the cylindrical green compact. The size of the die and sample can bee seen in the last session. Because of the symmetry, only half of the sample is considered. Bilinear axisymmetric elements such as CAX4 and DCAX4 have been used. A 30×40 element mesh is applied on the rectangular cross section area.

The compaction-sintering simulation consists of three problems: static pressing, heat transfer and creep. The first problem provides the initial density distribution and residual stress for sintering analysis. The history output of temperature field from the second problem has been written in ABAQUS result file and transferred into the sintering analysis as prescribed thermal conditions.

The porous elasticity model and modified Drucker-Prager/Cap plasticity model are used in the static pressing problem, which has three steps, as shown in Fig. 3. The parameters of Cap model are measured by Yi He[12]. Loose powder is compacted from apparent density to about 82% relative density, which is the initial density for the sintering simulation.

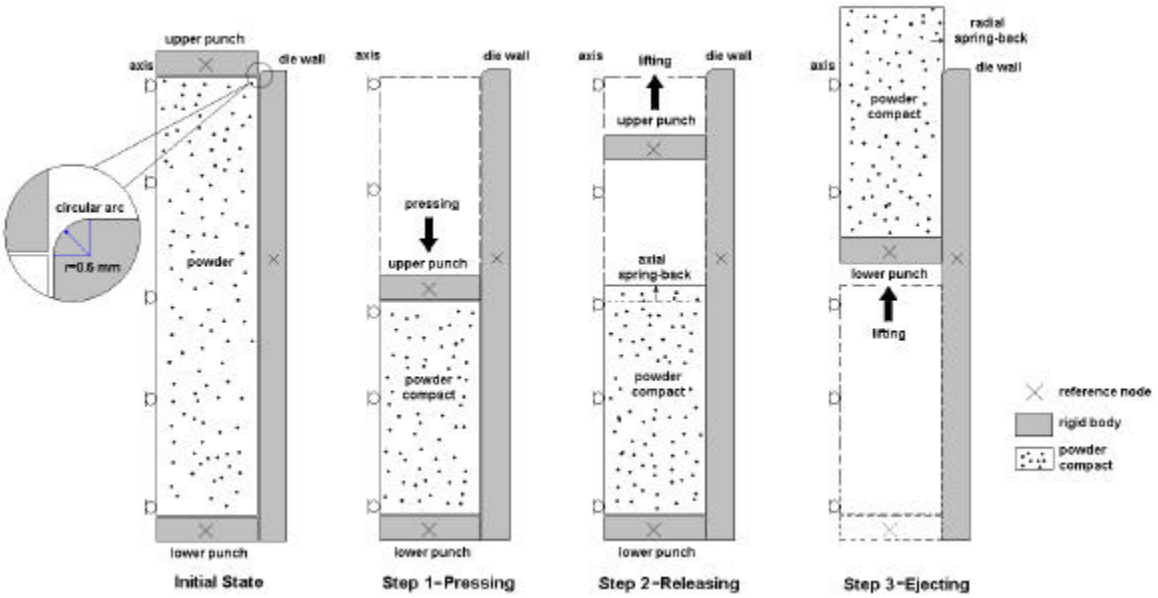

Fig. 3 Schematic picture on the one-punch pressing and spring-back problem

Sintering is a complex process with coinstantaneous changes of both thermal and mechanical problems. However, the couple temperature-displacement field analysis is usually too big and difficult to get converged. Thus a model with decoupled thermal and mechanical analysis has been tried and significant time saving has been achieved in this paper.

The elastic modulus of porous material, nominal elastic modulus E_n, will be smaller than that of the solid material. According to the investigation of elastic modulus with respect to porosity, the average porosity is very important and many attempts have been made to relate properties to this parameter. In this paper, however, it has been tested that the final result of sintering simulation is not sensitive to the elastic modulus. Thus a constant Young's modulus (69.3 GPa) is picked from [13]. Several other material parameters are also set as constants[14]. They are: Poisson's ratio=0.28, coefficient of thermal expansion=1.6×10^{-6} /K, and thermal conduction=14.6 W/(m·°C).

Grain growth plays a very important role during sintering. Large grain size will prohibit the densification. In the current sintering model, the driving force for sintering is proportional to the reciprocal of grain size. Based on different experiments, various empirical equations for grain growth have been found in the literature[15-18]. In the present work, the following equation is used to simulate the grain growth behavior during sintering.

$$\frac{dG}{dt} = \frac{A\exp(-Q_G / RT)}{G} \tag{23}$$

where G is the grain size. T is the absolute temperature. Q_G is the activation energy for grain growth, 280 kJ/mol. R is the universal gas constant, 8.314 J/K·mol. A is a constant parameter, 0.007 m^2/s.

RESULTS AND CONCLUSION

Fig.4 compares the predicted axial shrinkage curves of the three powder groups. All curves show that axial shrinkage is negative during the initial heating. This is because thermal expansion dominates the process at low temperature. The final shrinkage is comparatively small. For instance, it is around 2.5% for medium size powder compact, which means that the sintering is just in the initial to intermediate stage.

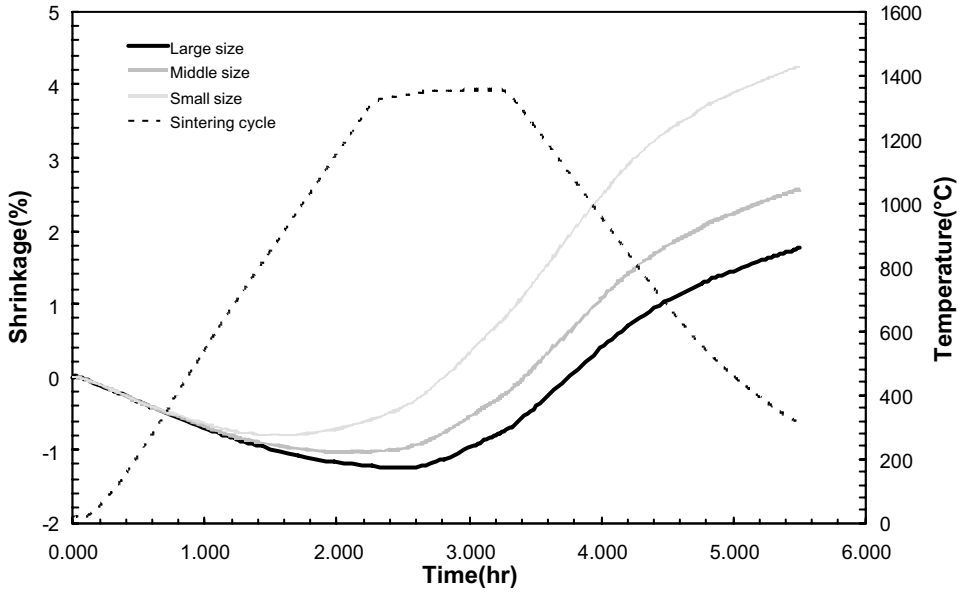

Fig.4 Simulation of axial shrinkage versus time for a stainless steel 316L presintered compact heated at a rate of 10°C/min to 1350°C in hydrogen

The comparison of density distribution between the presintered (range from 0.76 to 0.87) and sintered (range from 0.81 to 0.87) 316L samples determined by simulation can be seen in Fig.5.

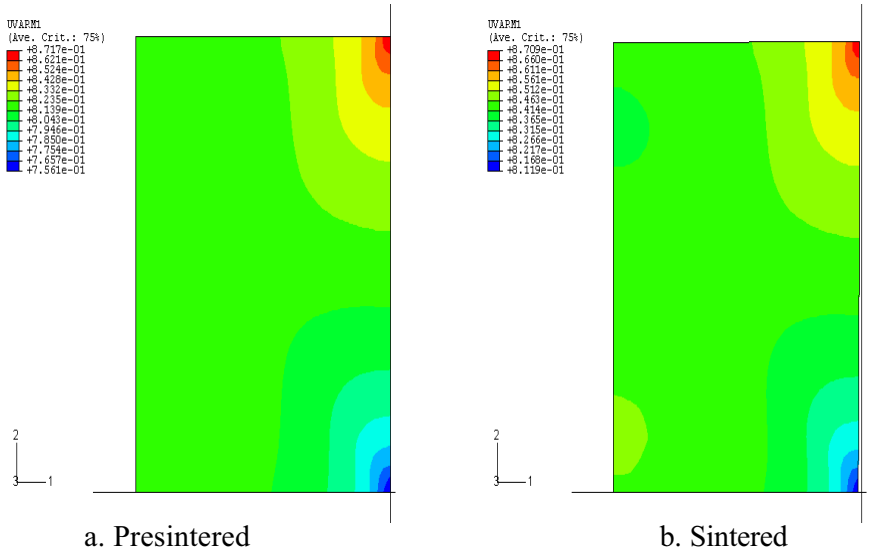

a. Presintered b. Sintered

Fig.5 Simulation result of relative density distribution on the cross section of the presintered and sintered stainless steel 316L cylinder compact (SS316L-Medium group)

Comparing Fig. 2 and 4, it can be found that the current sintering model is not so good at describing the behavior that the actual shrinkage starts immediately after the temperature gets to 1000°C. It can be seen that the simulation result is smaller than the test result when the temperature is higher than 1100°C, though the trend of both curves is the same.

From Fig. 5, we can see that the predicted density distribution pattern does not change so much after sintering. But the lower limit of density increases a lot, which means the lower density part of the sample has more shrinkage. This is true for the actual shrinkage behavior.

From the results above, it can be seen that a finite element model using an isotropic, linear-viscous constitutive law for a mixture of solid and voids, can describe the thermal mechanical behavior of powder compacts during the sintering process. The creep behavior was simulated by subroutines in ABAQUS and the shrinkage prediction is in a fair agreement with experimental data obtained by dilatometry.

REFERENCE

[1]. H. Riedel, “A Constitutive Model for the Finite-element Simulation of Sintering-Distortions and Stresses”, *Ceramic Powder Science III*, 1990, pp.619-630.
[2]. Eugene A. Olevsky, “Theory of sintering : from discrete to continuum”, *Mat. Sci. Engi. Rep.: A Review Journal*, R23, 1998, pp.41-100.
[3]. D. Z. Sun and H. Riedel, "Prediction of shape distortions of hard metal parts by numerical simulation of pressing and sintering", *Simulation of Materials Processing: Theory, Methods and Applications*, Shen & Dawson (eds), 1995, pp.881-886.
[4].H. Zipse, "Finite-Element Simulation of the Die Pressing and Sintering of a Ceramic Component", *Journal of the European Ceramic Society*, 17(14), 1997, pp.1707-1713.
[5]. K. T. Kim and Y. C. Jeon, "Densification behavior of 316L stainless steel powder under high temperature", *Materials Science and Engineering A245*, 1998, pp.64-71.

[6].O. Gillia and D. Bouvard, "Numerical Prediction of Shape Changes occurring during Sintering of Tungsten Carbide Parts", *1998 PM World Congress*, Special Interest Seminar-Fundamentals of Sintering
[7]. Gasik, M. and B. Zhang, "A constitutive model and FE simulation for the sintering process of powder compacts", *Computational Materials Science*, vol. 18, 2000, pp.93-101.
[8]. Riedel, H. and D.-Z. Sun, "Simulation of die pressing and sintering of powder metals, hard metals", *Numerical Methods in Industrial Forming Processes*, 1992, Chenot, Wood & Zienkiewicz (eds), pp.883-886.
[9]. E.A. Brandes, *Smithells Metals Reference Book*, 6th ed., Butterworth and Co., London, 1983
[10].R. M. German, "Supersolidus Liquid-Phase Sintering of Prealloyed Powders", *Metallurgical and Materials Transactions A ,*28A, 1997, pp.1553-1567.
[11]. ABAQUS/Standard User's Manual, Vol. III, Version 6.2, pp.24.2-1—24.2-12.
[12]. Y. He, "Numerical Simulation for 316L Stainless Steel Powder Die Compaction", 2002, M.S. Thesis, Pennsylvania State University, University Park, PA.
[13]. German, R. M. (1994). "Compact Characterization", *Powder Metallurgy Science*, 384. Label: 0059
[14]. Powder Metallurgy, ASM Handbook, Vol.7, 1990
[15]. M. F. Ashby, K. E. E. (1982). "A first report on diagrams for grain growth in welds." *Acta Metall*. 30(11-a): 1969-1978.
[16]. Kashyap, B. P. T., K. (1992). "Grain growth behaviour of type 316L stainless steel." *Materials Science & Engineering A: Structural Materials: Properties, Microstructure and Processing* A149(2): L13-L16.
[17]. Chidiac se, W. D., Mirza Fa (1992). "Finite-element modeling of transient heat-transfer and microstructural evolution in welds .2. modeling of grain-growth in austenitic stainless-steels." *Metallurgical Transactions B-Process Metallurgy* 23b(6): 841-845.
[18]. Y. S. Kwon, S. H. C., H. K. Ahn, S. T. Chung, S. J. Park, and D. T-S. Yoon (2001). "CAE analysis for sintering stage of powder injection molding", *2001 International Conference on Powder Metallurgy & Particulate Materials*, New Orleans, LA, MPIF.